ARL-TR-7763● SEP 2016

US Army Research Laboratory

Photoionization in a Numerical Simulation of a Spark Discharge in Air

by Charles R Hummer

NOTICES

Disclaimers

The findings in this report are not to be construed as an official Department of the Army position unless so designated by other authorized documents.

Citation of manufacturer's or trade names does not constitute an official endorsement or approval of the use thereof.

Destroy this report when it is no longer needed. Do not return it to the originator.

ARL-TR-7763 ● SEP 2016

US Army Research Laboratory

Photoionization in a Numerical Simulation of a Spark Discharge in Air

by Charles R Hummer
Weapons and Materials Research Directorate, ARL

REPORT DOCUMENTATION PAGE

Form Approved
OMB No. 0704-0188

1. REPORT DATE *(DD-MM-YYYY)*	2. REPORT TYPE	3. DATES COVERED (From - To)
September 2016	Technical Report	1–31 January 2015

4. TITLE AND SUBTITLE
Photoionization in a Numerical Simulation of a Spark Discharge in Air

5a. CONTRACT NUMBER

5b. GRANT NUMBER

5c. PROGRAM ELEMENT NUMBER

6. AUTHOR(S)
Charles R Hummer

5d. PROJECT NUMBER

5e. TASK NUMBER

5f. WORK UNIT NUMBER

7. PERFORMING ORGANIZATION NAME(S) AND ADDRESS(ES)
US Army Research Laboratory
ATTN: RDRL-WMP
Aberdeen Proving Ground, MD 21005-5069

8. PERFORMING ORGANIZATION REPORT NUMBER
ARL-TR-7763

9. SPONSORING/MONITORING AGENCY NAME(S) AND ADDRESS(ES)

10. SPONSOR/MONITOR'S ACRONYM(S)

11. SPONSOR/MONITOR'S REPORT NUMBER(S)

12. DISTRIBUTION/AVAILABILITY STATEMENT
Approved for public release; distribution is unlimited.

13. SUPPLEMENTARY NOTES

14. ABSTRACT
Lightning is an example of an electric discharge in air. These electric discharges can heat the air to very high temperatures and become an intense source of ultraviolet light that can photoionize the ambient air. This produces energetic free electrons in the air, making it conductive to electric current and thus may change the dynamics of the discharge. This has not been included in previous theoretical studies and numerical simulations. A detailed development of a numerical simulation is first presented without photoionization, reproducing previous works. When photoionization was included, there was only a small difference in the radius of the discharge over time. The position of the shock wave and its peak pressure over time were also nearly the same in both cases. Photoionization, however, did result in a decrease of the arc's core temperature and an increase in its electrical conductivity. Since the measurement of the core temperature is difficult, the only accessible measurement is electrical conductivity, which can evaluate the importance of photoionization.

15. SUBJECT TERMS
spark discharge, air, pulse power, photoionization, electrical conductivity

16. SECURITY CLASSIFICATION OF:			17. LIMITATION OF ABSTRACT	18. NUMBER OF PAGES	19a. NAME OF RESPONSIBLE PERSON
a. REPORT	b. ABSTRACT	c. THIS PAGE			Charles R Hummer
Unclassified	Unclassified	Unclassified	UU	42	19b. TELEPHONE NUMBER (Include area code) 410-278-5680

Contents

List of Figures

List of Tables

1. Introduction

The electrical characteristics of an arc that is produced by a high-current pulse have been studied for spark gap switches, lightning and thunder, exploding thin conductors, and ignition of a fuel/air mixture in an internal combustion engine. All of these arcs have a circular cylindrical channel of an expanding gas that is nearly completely ionized at a high temperature and low density. Under these conditions, the channel conducts nearly all of the electrical current. The ambient air conducts very little electrical current, but there is a cylindrical shock wave expanding through it. Flash lamps have all these features except for an expanding shock wave in the air. The general approach taken by the early calculations was to assume that the channel had a uniform temperature, pressure, current density, and electrical conductivity. Nearly all of these theories assume that the channel has an initial radius or implies that there is one. They also imply that the total mass of the gas in the initial channel is constant. Various approximations were then used to solve the equations of motion of the gas for the radius of the channel and the resistance of the arc as functions of time.

Engel et al.[1] reviewed these calculations and compared them with the experimental results by Akiyama et al.,[2] who measured the current for arcs through air at various pressures and arc lengths. The resistances for the arcs were then calculated from the current and a circuit model of the experiment. The resistance was high at the start of the arc, decreased to a minimum near the peak current, and slowly increased afterward. Engel chose one of the results for comparison with a number of theories. Most of the reviewed theories approximated the resistance of the arc up to about the peak current. Some of the theories had to be scaled, but some of the scaling may not be justified. Most of the reviewed theories gave a resistance that continued to decrease after the maximum current. The few theories that gave an increasing resistance did not increase as much as the experimental result. An agreement for the resistance at all times was achieved by combining 1) Engel's proposed equation for time dependence of the radius that is an integral of a function of the current and 2) an equation in one of the reviewed theories[3] that gave the resistance of the arc as a function of the current. A close examination of the current and the circuit model used by Akiyama et al.[2] to derive the arc resistance, however, showed that this arc resistance can be questioned.

A detailed numerical study of an arc came from the research on thunder and lightning.[4] This study is an extension of an earlier finite element model for shock waves from a line source,[5] where the hydrodynamic equations that include a pseudoviscous term[6] for the formation of a shock wave were numerically solved.

These equations were extended by adding a term to the energy balance equation that is a sum of the energy added to or lost from a finite element[4] by various processes: Joule heating, thermal conductivity, radiation emitted by the finite element, and the radiation absorbed from the rest of the finite elements. This work was later reviewed by Akram and Lundgren[7] and by a continued publication, Akram,[8] which used a slightly different set of finite difference equations and a slightly different equation of state for air. The equations for the thermal conductivity of air and the electrical conductivity of air are the same as Plooster's.[4] Unfortunately, the equation of state for air and the equation for the electrical conductivity of air in Akram and Lundgren[7] have typographical errors, both of which are corrected here. Plooster[4] uses an equation for the electrical conductivity of air that was a modification by Olsen[9] for atmospheric-pressure plasmas from an expression for an ionized gas by Spitzer and Harm.[10] After referring to Olsen,[9] however, the modification was not clearly stated. There were changes in notation and possible typographical errors. In addition, the subject of radiation transport, where the black body radiation from one finite element is absorbed and heats a distant finite element, was not explained very well in Plooster[4] and Akram and Lundgren.[7]

A detailed description of the Lagrangian hydrodynamic equations for the finite elements are developed and presented here and are different from those of Plooster[4] and Akram and Lundgren.[7] The equation of state for air, the electrical conductivity of air, and a modified equation for the pseudoviscosity are also discussed in detail. It is assumed that the energy transport from one finite element to the others is by photoionization, where the ultraviolet light ionizes the neutral atoms in a finite element. The addition of the energetic electrons and their density increases the electrical conductivity of the finite element. The bound-bound and free-free radiative transfer processes present in a plasma that is in local thermal equilibrium are ignored.[11–13] It is assumed that these processes have little effect on the electrical conductivity. The free-bound process where a free electron recombines with an ion by emitting a photon is included by using a rough estimation. These equations were solved for the assumed current profile used by Plooster[4] and Akram and Lundgren[7] both when there is no photoionization and when there is photoionization. The temperature and pressure at the very center of the arc, the radius of the arc, and the position of the shock wave versus time are then compared with Akram and Lundgren's[7] results.

2. Hydrodynamic Equations

In the Lagrangian description for a 1-D cylindrical coordinates, let the initial radial position of a very small portion of the gas be x. At some later time, this small portion

of the gas is moved to a new location *r(x,t)*. This portion then has a velocity *u(r(x,t))*, a density *ρ(r(x,t))*, a pressure *p(r(x,t))*, and an internal specific energy *ε(r(x,t))* in units of energy per unit mass, which all follow a set of differential equations. In some of these equations, however, it is convenient to use the specific volume *v* that is simply the reciprocal of the density, $v = 1/\rho$. The differential equations for these quantities are found from the conservation of mass,

$$v\big(r(x,t)\big) = v_o \frac{r(x,t)}{x}\frac{\partial r(x,t)}{\partial x}, \tag{1}$$

the conservation of momentum,

$$\frac{\partial u(x,t)}{\partial t} = -v_o \frac{\partial\big(p(r(x,t)) + q(r(x,t))\big)}{\partial x}\frac{r(x,t)}{x}, \tag{2}$$

and the conservation of energy,

$$\frac{\partial \varepsilon(\rho(r(x,t)),T(r(x,t))}{\partial t} = -\big(p(\rho(r(x,t)),T(r(x,t)) + q(r(x,t)\big)\frac{\partial v\big(r(x,t)\big)}{\partial t} + W, \tag{3}$$

where *W* is the power per unit mass from Joule heating, radiation loss and gain, thermal conduction, and so forth. The velocity is simply

$$u(x,t) = \frac{\partial r(x,t)}{\partial t}, \tag{4}$$

and *T(r(x,t))* is the temperature. v_o is the specific volume of the ambient air that is uniform at the beginning. The term *q(r(x,t))* is the pseudoviscosity term[6]

$$q = \rho(\rho_o c\Delta x)^2\left(\frac{\partial v}{\partial t}\right)^2 \; when \; \frac{\partial v}{\partial t} < 0$$

or

$$q = 0 \; when \; \frac{\partial v}{\partial t} \geq 0, \tag{5}$$

where *c* is a constant with no units that is on the order of unity. When this constant is increased, the width of the shock wave front is spread out over a number of grid points and smoothes out some of oscillations near the front. A value of about 1.4 was used in the following results. This expression for the pseudoviscous term is not convenient to use for the finite difference equations that are forward in time and centered in space.[14] In this scheme, the values of the position *r(x,t)*, velocity *u(x,t)*, specific volume *v(x,t)*, specific internal energy *ε(x,t)*, and pressure *p(x,t)* are used to advance their values to a short time step forward *Δt*: *r(x,t+Δt)*, *u(x,t+Δt)*, *v(x,t+Δt)*, *ε(x,t+Δt)*, and *p(x,t+Δt)*. The time derivative of the specific volume as it stands depends on its known present value and its unknown future value. It can be expressed, however, in terms of the known distribution in space of variables at a given time by starting with the time derivative of the conservation of mass equation

$$\frac{\partial v}{\partial t} = \frac{1}{\rho_o x}\left[\frac{\partial r}{\partial t}\frac{\partial r}{\partial x} + r\frac{\partial^2 r}{\partial t \partial x}\right] = \frac{1}{\rho_o x}\left[u\frac{\partial r}{\partial x} + r\frac{\partial u}{\partial x}\right] = \frac{1}{\rho_o}\frac{\partial (ru)}{\partial x} \tag{6}$$

to give

$$q = \rho\left(\frac{c\Delta x}{x}\right)^2\left(\frac{\partial (ru)}{\partial x}\right)^2 \text{ when } \frac{\partial (ru)}{\partial x} < 0 \;\; or \;\; q = 0 \text{ when } \frac{\partial (ru)}{\partial x} \geq 0. \tag{7}$$

A common convention in writing the finite difference equations is to give a superscript and a subscript of integers to the variables for the boundary between the elements, as shown in Fig. 1, where r_j^n is the position of the boundary, u_j^n is the velocity of the boundary, and f_j^n is a flux that is crossing the boundary. The flux can be a heat flux or a radiation flux as examples. The superscript means that the time for these variables is at the *n*th time step, and the subscript means that the variables began at the *j*th starting position. If the starting positions are evenly spaced by Δx, r_j^n is equivalent to $r(j\,\Delta x, t_n)$, and the position at the next time step r_j^{n+1} is equivalent to $r(j\,\Delta x, t_n+\Delta t_n)$, or $r(j\,\Delta x, t_{n+1})$ for the next time step. The starting positions x_j do not have a superscript because they do not change with time. The positions r_j^n and r_{j+1}^n define the boundaries for an element of gas with intrinsic properties, which are conventionally indicated by a subscript with an added half integer in Fig. 1: the pressure $p_{j+1/2}^n$, temperature $T_{j+1/2}^n$, density $\rho_{j+1/2}^n$, specific internal energy $\varepsilon_{j+1/2}^n$, and thermal conductivity $\kappa_{j+1/2}^n$.

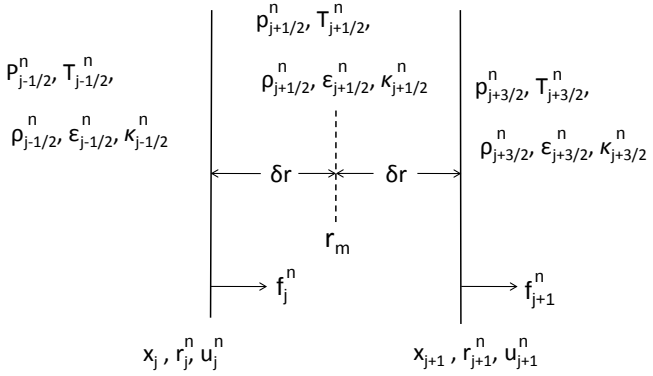

Fig. 1 Notation used for the finite difference equations

The finite difference equations are used in the following sequence. The velocity, position, and density are first stepped forward in time:

$$u_j^{n+1} = u_j^n + \frac{v_o}{\Delta x}\frac{r_j^n}{x_n}\left[p_{j-1/2}^n - p_{j+1/2}^n + q_{j-1/2}^n - q_{j+1/2}^n\right]. \tag{8}$$

$$r_j^{n+1} = r_j^n + \Delta t_n u_j^{n+1}. \tag{9}$$

$$\rho_{j+1/2}^{n+1} = \frac{1}{v_j^{n+1}} = \rho_o \frac{\left(x_{j+1}\right)^2 - \left(x_j\right)^2}{\left(r_{j+1}^{n+1}\right)^2 - \left(r_j^{n+1}\right)^2}. \quad (10)$$

$$\rho_{j+\frac{1}{2}}^{n+1} = \frac{1}{v_j^{n+1}} = \rho_o \frac{\left(x_{j+1}\right)^2 - \left(x_j\right)^2}{\left(r_{j+1}^{n+1}\right)^2 - \left(r_j^{n+1}\right)^2}. \quad (11)$$

Next, the pseudoviscosity is stepped forward in time:

$$q_{j+1/2}^{n+1} = \left(\frac{\rho_{j+1/2}^{n+1} + \rho_{j+1/2}^{n}}{2}\right)\left(\frac{2c\left(r_{j+1}^{n+1}u_{j+1}^{n+1} - r_j^{n+1}u_j^{n+1}\right)}{x_{j+1} + x_j}\right)^2 \text{ when } r_{j+1}^{n+1}u_{j+1}^{n+1} - r_j^{n+1}u_j^{n+1} < 0 \quad (12)$$

and

$$q_{j+1/2}^{n+1} = 0 \text{ when } r_{j+1}^{n+1}u_{j+1}^{n+1} - r_j^{n+1}u_j^{n+1} \geq 0. \quad (13)$$

Finally, a transcendental equation must be numerically solved for the new temperature.

$$\begin{aligned}\left(T_{j+1/2}^{n+1}, \rho_{j+1/2}^{n+1}\right) + p\left(T_{j+1/2}^{n+1}, \rho_{j+1/2}^{n+1}\right)\left(\frac{r_{j+1}^{n+1}u_{j+1}^{n+1} - r_j^{n+1}u_j^{n+1}}{\rho_o \Delta x}\right) &= \varepsilon\left(T_{j+1/2}^{n}, \rho_{j+1/2}^{n}\right) \\ -q_{j+1/2}^{n+1}\left(\frac{r_{j+1}^{n+1}u_{j+1}^{n+1} - r_j^{n+1}u_j^{n+1}}{\rho_o \Delta x}\right) + \Delta t_n W_{j+1/2}\end{aligned} \quad . \quad (14)$$

The function $p(T,\rho)$ (Eq. 30) is the thermal equation of state, and the function $\varepsilon(T,\rho)$ (Eq. 29) is the caloric equation of state for the gas; more details of these functions will be given later. If the gas is ideal, these equations are simple and easily solved for T_j^{n+1}. If the gas is real, however, these equations may not be solved in closed form for the new temperature. Instead, the old temperature T_j^n serves as a first guess for the new temperature, and the equation is tested for equality. Based on the results of this test, another temperature is judiciously chosen and tested. By using the mean value theorem and testing for equality, an acceptable range for the temperature can be found in which there is equality. A temperature within this range is chosen for $T_{j+1/2}^{n+1}$ to find the new specific energy

$$\varepsilon_{j+1/2}^{n+1} = \varepsilon\left(T_{j+1/2}^{n+1}, \rho_{j+1/2}^{n+1}\right) \quad (15)$$

and the new pressure

$$p_{j+1/2}^{n+1} = p\left(T_{j+1/2}^{n+1}, \rho_{j+1/2}^{n+1}\right). \quad (16)$$

These new values are then used for the next time step.

The value for the time step Δt_n has limits. These difference equations become unstable if Δt_n is too large. If Δt_n is too small, the computation time for a total solution over a range of time increases. Plooster[15] used the stability relation given by Richtmyer and Morton,[16]

$$\Delta t_j \leq \frac{1}{4\alpha^2}\frac{r_{j+1}-r_j}{u_j-u_{j+1}}, \tag{17}$$

where α is a parameter that originated from the pseudoviscosity. This condition has a simple interpretation. The numerator is the spacing between 2 positions. The denominator is the closing velocity of the 2 positions when $u_j > u_{j+1}$. Thus, this fraction is the additional time when the distance between the 2 positions is zero if they continue to move at their velocities. This cannot happen because the positions represent material that cannot pass through another and result in a negative width for the element. If both velocities are zero or if $u_j < u_{j+1}$ for an expanding element, then the time step is taken to be

$$\Delta t_j \leq \frac{1}{4\alpha^2}\frac{r_{j+1}-r_j}{s_{j+1/2}}, \tag{18}$$

where $s_{j+1/2} = \sqrt{\gamma p_{j+1/2} / d_{j+1/2}}$ is the local speed of sound with γ = 1.4. Because each element has a different time, all the elements must be examined for a minimum time, and the time step is set to a fraction of this time. A value for α that is taken to be independent here from the constant *c* in Eq. 5 can be found with some trial and error, but $\alpha = 1$ was sufficient for the following calculations.

In the conservation of energy equation, the *W* term is the sum of the energy per unit time per mass that is added or lost by the element $W_{j+1/2} = W_{Joule} - W_{bb} + W_{therm}$. W_{Joule} is the Joule or ohmic heating.

$$W_{Joule} = E^2 \frac{\sigma_{j+1/2}}{\rho_{j+1/2}}. \tag{19}$$

E is the common electric field for all the elements that is given by the total current divided by the sum of the products of the electrical conductivity and the cross sectional area of all the elements.

$$E = \frac{I(t)}{\sum \sigma_{j+\frac{1}{2}} a_j}, \tag{20}$$

where $a_j = \pi\left(r_{j+1}^2 - r_j^2\right)$ and the total current[4,7] is assumed to be

$$I(t) = 4.0 \times 10^4(\exp(-4.0 \times 10^4 t) - \exp(-4.0 \times 10^5 t)). \tag{21}$$

The maximum for this current is about 27.9 kA at about 6.4 μs. The power loss from the black body radiation according to Plooster[4] is $Q_{bb} = 4\sigma_{sb}T^4 k_b$. The term $4\sigma_{sb}T^4$ is the integral of the spectral radiation intensity over all the frequency and solid angle, where σ_{sb} is the Stefan-Boltzmann constant and k_b is an absorption constant that was arbitrarily chosen to be 1.0 cm^{-1} in the gas at the ambient density. Thus, the specific power loss per unit mass

$$W_{bb} = \frac{4\sigma_{sb}T^4\ 1.0}{\rho_o}. \tag{22}$$

W_{therm} is the heat conducted into an element from its neighbors. According to Akram and Lundgren,[7] W_{therm} in differential form is

$$W_{therm} = \frac{1}{\rho_o^2 x}\frac{\partial}{\partial x}\left(\frac{\kappa\rho r^2}{x}\frac{\partial T}{\partial x}\right). \tag{23}$$

κ is the heat conductivity of the element. Casting this differential expression into a finite difference form is not obvious because it calls for a differentiation of a product of the intrinsic quantities T, ρ, and κ with a spatial variable x. Transforming the partial derivatives with respect to x into the partial derivatives with respect to r, however, gives a simpler differential that is easier to interpret. Using the conservation of mass, the operator

$$\frac{\partial}{\partial x} = \frac{\rho_o}{\rho}\frac{x}{r}\frac{\partial}{\partial r} \tag{24}$$

is used to express Eq. 23 as the familiar radial component of the heat conduction equation in cylindrical coordinates

$$W_{therm} = \frac{1}{\rho}\left[\frac{1}{r}\frac{\partial}{\partial r}\left(\kappa r\frac{\partial T}{\partial r}\right)\right], \tag{25}$$

where the expression in the parenthesis is the radial component of the heat flux vector $\vec{h} = -\kappa\nabla T$, and the expression in the brackets is the radial component of the divergence of the heat flux. This suggests a way to translate this equation to the finite elements. Let $h_j = \kappa\frac{T_{j-1/2}-T_{j+1/2}}{\delta r}$ be the heat flux entering the element on the left, where it is assumed that the temperature at r_j is $T_{j\text{-}1/2}$ and the temperature at r_m, $r_m = (r_{j+1} + r_j)/2$, is $T_{j+1/2}$. The heat flux leaving the element on the right is $h_{j+1} = \kappa\frac{T_{j+1/2}-T_{j+3/2}}{\delta r}$, where it is assumed that the temperature at r_{j+1} is $T_{j+3/2}$. After multiplying the fluxes by their areas, the total heat entering the element is

$$Q_j = \frac{\kappa_j}{\delta r_j}\left[2\pi r_j\left(T_{j-1/2} - T_{j+1/2}\right) - 2\pi r_{j+1}\left(T_{j+1/2} - T_{j+3/2}\right)\right]. \tag{26}$$

This is then divided by the mass within the element for the specific heat W_{therm},

$$W_{therm} = \frac{Q_j}{\rho_j 2\pi r_m 2\delta r} = \frac{\kappa_j}{\rho_j 4\pi r_m \delta r^2}\left[2\pi r_j\left(T_{j-1/2} - T_{j+1/2}\right) - 2\pi r_{j+1}\left(T_{j+1/2} - T_{j+3/2}\right)\right]. \quad (27)$$

After applying $r_j = r_m - \delta r$ and $r_{j+1} = r_m + \delta r$, this can be written as

$$W_{therm} = \frac{\kappa_j}{2\rho_j}\left[\frac{T_{j+\frac{3}{2}} + T_{j-\frac{1}{2}} - 2T_{j+\frac{1}{2}}}{\delta r^2} + \frac{T_{j+\frac{3}{2}} - T_{j-\frac{1}{2}}}{r_m \delta r}\right]. \quad (28)$$

The thermal conductivity in units of erg cm^{-1} sec^{-1} deg^{-1} is a sum of 3 terms.[4,7]

$$\kappa = 0.1488\sigma T + 2.2\times10^{13}\rho\frac{dA_0}{dT} + 1000\left(1 - A_1\right)T^{1/2}. \quad (29)$$

The first term is the thermal conductivity by the electrons determined from the Wiedermann-Franz law, where σ is the electrical conductivity. The second term is from the diffusion of the recombination energy, where A_0 is from Eq. 32 (Section 3). The last term is the contribution from the neutral particles, where $(1-A_1)$ is the fraction of neutral particles and A_1 is also from Eq. 32 (Section 3).

The correct initial conditions for an arc at the very beginning of a current pulse are speculative, but Plooster[4] proposed 2 different initial conditions. Even though these conditions may not be correct, it is hoped that the results would not depend on the exact initial conditions at later times. One initial condition has a channel of gas at ambient pressure with an assumed radius and high temperature. These conditions may occur just prior to the main discharge of a lightning stroke when a large current flows between the ground and the cloud. Just before the main discharge, there are leading strokes emitting from the ground to the cloud and other leading strokes emitting from the cloud to the ground. These leading strokes propagate toward each other until they make contact, initiating the main discharge. This also occurs between clouds. It is assumed that these leading strokes heat a channel of air at atmospheric pressure. The other initial condition has a channel of gas at the ambient density with an assumed radius and high temperature, which may occur when an arc is formed so quickly that the gas has yet to move. This condition implies that the gas was heated by a current for some time before the gas is allowed to move. Plooster[4] and Akram and Lundgren[7] ignore this initial current, and simply start from zero current and allow the gas to move at the same time. From Akram and Lundgren's graphs,[7] the initial temperature for the channel was 15,000 K but its initial radius was not stated. An initial radius of 0.1 cm, however, gave comparable results.

Using Akram's[8] and Plooster's[4] equations for the electrical conductivity of air (Eqs. 36 and 37; Section 3) Akram's[8] corrected equation of state for air (Eqs. 30, 31, and 32; Section 3), and assuming that the channel is air at ambient density uniformly heated to a temperature of 15,000 K within a radius of 0.1 cm, these finite

difference equations were solved without radiation transfer. At the time 6.4 μs for the maximum current 27.9 kA, the results gave the distribution of the temperature (Fig. 2), pressure (Fig. 3), density (Fig. 4), and current density (Fig. 5). It is remarkable that all of these quantities are fairly uniform within the channel radius of about 0.82 cm and that a shock wave that is the peak in the pressure at 1.1 cm in Fig. 3 is already at some distance from the channel. This supports the assumptions used in the earlier models.

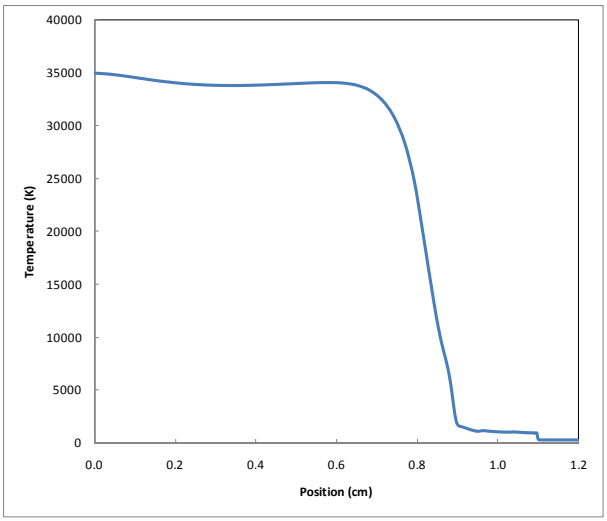

Fig. 2 Temperature vs. position at 6.4 μs

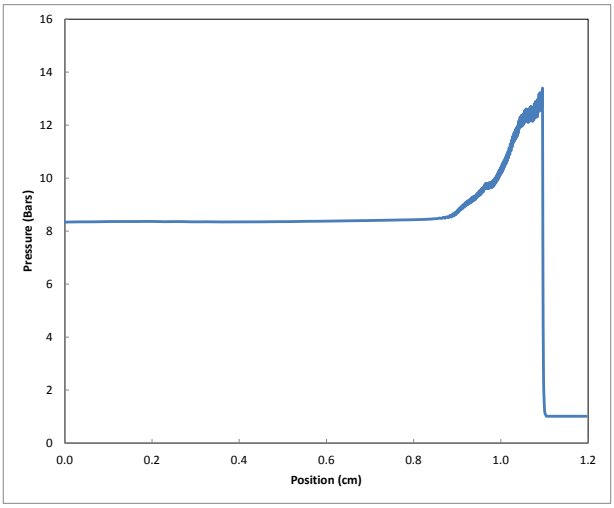

Fig. 3 Pressure vs. position at 6.4 μs

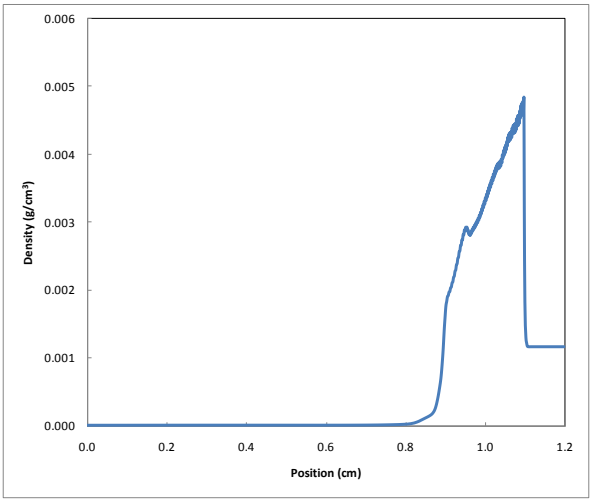

Fig. 4 Density vs. position at 6.4 μs

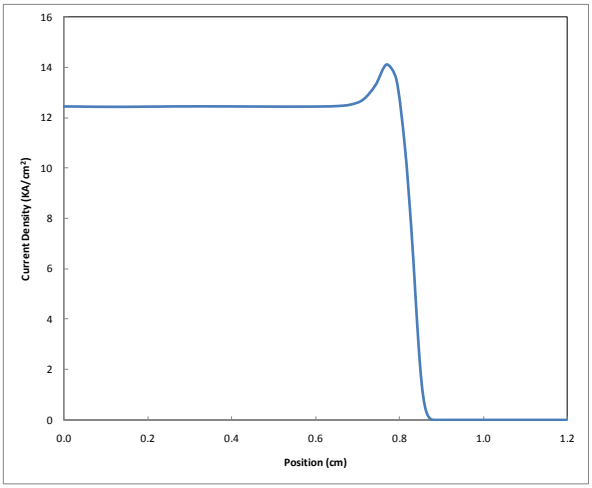

Fig. 5 Current density vs. position at 6.4 μs

3. Equation of State for Air

The pressure of air as a function of its temperature and its density is the thermal equation of state,[5]

$$p(T,\rho) = \rho RT[1 + A_0 + 2(A_1 + A_2)], \tag{30}$$

and the specific internal energy of air in ergs per gram is calculated by the caloric equation

$$\varepsilon(T,\rho) = RT\big(5 + A_0/2 + 3(A_1 + A_2)\big) + A_0 I_0 + A_1 I_1 + A_2 I_2. \tag{31}$$

In these equations, A_0 is the fraction of the molecules that are dissociated: $A_0 = 0$ when there are no dissociated molecules and $A_0 = 1$ when all the molecules are dissociated. A_1 is the fraction of the atoms that are singly ionized: $A_1 = 0$ when none of the atoms are singly ionized and $A_1 = 1$ when all the atoms are singly ionized. A_2 is the fraction of the singly charged ions that become doubly charged: $A_2 = 0$ when none of the singly charge ions is doubly charged and $A_2 = 1$ when all of the singly charged ions are now doubly charged. A_0, A_1, and A_2 are functions of the temperature and density found by applying the Saha equation[13] for the local thermal equilibrium between 2 states separated by an energy. In this case, the lower energy state for A_0 is the molecule, and the higher energy state is when the molecule dissociates into atoms. The lower energy state for A_1 is the atom, and the higher energy state is the singly charged ion. The lower energy state for A_2 is the singly charged ion, and the higher energy state is the doubly charged ion. After correcting a typographical error, these fractions, according to Akram and Lundgren,[7] are

$$\begin{aligned}
A_0 &= 2\left[1+\sqrt{1+2B_0}\right]^{-1} \\
B_0 &= \frac{C_0\rho}{\sqrt{T}}\frac{exp\left(\frac{I_0}{\Re T}\right)}{1-\exp\left(-T_v/T\right)} \\
A_1 &= 2\left[1+\sqrt{1+2B_1}\right]^{-1} \\
B_1 &= \frac{C_1\rho}{T^{3/2}}\exp\left(\frac{I_1}{2\Re T}\right) \\
A_2 &= 2\left[1+B_2+\sqrt{1+6B_2+B_2^2}\right]^{-1} \\
B_2 &= \frac{C_2\rho}{T^{3/2}}exp\left(\frac{I_2}{2\Re T}\right)
\end{aligned} \quad . \tag{32}$$

The values I_0, I_1, I_2 and C_0, C_1, C_2 in the Table are from Akram[8] for an air that has properties that are a weighted sum of the corresponding property of a gas with a ratio in number of 0.788 N_2 and 0.212 O_2. Compounds of nitrogen and oxygen and their ions that may form in and around the arc are ignored: NO, NO^+, O_3, and so forth. The trace atmospheric gasses are also ignored: argon, carbon dioxide, and so forth.

Table Constants for the equation of state from Akram.[8] The gas constant per gram is the universal gas constant divided by the molecular weight.

Parameter name	Symbol	Value	Units
Molecular weight	Mw	28.86	g/mole
Gas constant per gram	*R*	2.880946×10^{6}	erg/K/g
Specific dissociation energy	I0	2.930557×10^{11}	erg/g
Specific first-ionization energy	I1	9.591766×10^{11}	erg/g
Specific second-ionization energy	I2	2.062056×10^{12}	erg/g
Saha's constant for dissociation	C0	4.817588×10^{-1}	$cm^3K^{3/2}/g$
Saha's constant for first-ionization	C1	1.101416×10^{7}	$cm^3K^{3/2}/g$
Saha's constant for second-ionization	C2	1.033965×10^{7}	cm3K3/2/g
Vibration temperature	Tv	3150	K
Ambient temperature	To	300	K
Ambient pressure	po	1.01325×10^{6}	$dyne/cm^2$
Ambient density	ρo	1.172358×10^{-3}	g/cm^3

The electrical conductivity of the gas depends on the number density of the electrons n_e, number density of the neutral "air atoms" n_0, number density of the singly charged ions n_1, and number density of the doubly charged ions n_2. These number densities are related to the fractions A_0, A_1, and A_2 but they are not for a given number density of "air atoms" N where $N = Av\ \rho/14.43$. Av is Avogadro's number, and 14.43 is half of the molecular weight for the "diatomic gas Air_2": 28.86. In terms of these fractions, the number densities are $n_m = (1 - A_0)N/2$ for molecules, $n_a = A_0(1 - A_1)N$ for atoms, $n_0 = 2n_m + n_a = (1 - A_0A_1)N$ for the total number of atoms that are associated in molecules and atoms that are dissociated, $n_1 = A_0\ A_1\ (1 - A_2)\ N$ for singly charged ions, and $n_2 = A_0\ A_1\ A_2\ N$ for doubly charged ions. Note that $N = n_0 + n_1 + n_2$. Thus, the number of electrons is $n_e = 1\ n_1 + 2\ n_2 = A_0\ A_1\ (1 + A_2)N$, and the total number of ions is $n_+ = n_1 + n_2 = A_0\ A_1N$. The mean ionic charge that will be used in the equation for the electrical conductivity is defined as

$$Z = \frac{1}{n_e}\sum_{j=1} n_j Z_j^2\ , \tag{33}$$

where Z_j is the charge of the ion ($Z_1 = 1$, $Z_2 = 2$, etc.) and n_j's are their respective number densities. In terms of the fractions, the mean ionic charge up to the doubly charged ions is

$$Z = \frac{1n_1 + 2^2 n_2}{n_e} = \frac{A_0A_1\left(1 - A_2\right) + 4A_0A_1A_2}{A_0A_1\left(1 + A_2\right)} = \frac{\left(1 + 3A_2\right)}{\left(1 + A_2\right)}\ . \tag{34}$$

Because of the energy dependence of A_0, A_1, and A_2, most of the atoms are singly charged before there are doubly charged ions. Also, most of the molecules are dissociated into atoms before there are singly charged ions. Thus, the following are very good approximations that are used by Plooster[4] and Akram and Lundgren[7]: $n_e = A_0 A_1 (1 + A_2)N \approx (A1 + A2)N$, $n_+ = A_0 A_1 N \approx A_1 N$, $n_0 = (1 - A_0 A_1)N \approx (1 - A_1)N$, and

$$Z = \frac{\left(1+3A_2\right)}{\left(1+A_2\right)} \approx \frac{A_1+3A_2}{A_1+A_2}. \tag{35}$$

4. Electrical Conductivity of Gasses

The electrical conductivity used by Plooster[4] and Akram and Lundgren[7] in Siemens per centimeter (S/cm) is

$$\sigma = \frac{4.173\times10^{-10}\left(A_1+A_2\right)T^{-\frac{1}{2}}}{2.0\times10^{-15}\left(1-A_1\right)+A_1\left\langle a_i\right\rangle_{Av}}, \tag{36}$$

where the average electron-ion cross section $\langle a_i \rangle_{Av}$ is given by

$$\left\langle a_i\right\rangle_{Av} = \frac{2.8\times10^{-6}}{T^2}\left[\frac{A_1+3A_2}{A_1+A_2}\right]^2 Ln\left\{\frac{1.727\times10^{-5}T}{\left(A_1\rho\right)^{1/3}}\left[\frac{A_1+A_2}{A_1+3A_2}\right]\right\}. \tag{37}$$

Using the approximations for n_e, n_0, and n_+ from the equation of state, these equations are

$$\sigma = \frac{4.173\times10^{-10}n_eT^{-\frac{1}{2}}}{2.0\times10^{-15}n_n+n_+\left\langle a_i\right\rangle_{Av}} \tag{38}$$

and

$$\left\langle a_i\right\rangle_{Av} = \frac{2.8\times10^{-6}Z^2}{T^2}Ln\left\{\frac{1.727\times10^{-5}T}{\left(A_1\rho\right)^{1/3}Z}\right\}. \tag{39}$$

Plooster[4] simply states that this equation is a modification by Olsen[9] of the electrical conductivity for an ionized gas of Spitzer and Harm[10] for atmospheric-pressure plasmas. Olsen did not provide any explanation for the modifications. Also, there were some typographical errors, changes in notation, choice for some terms, and possible omissions. Thus, another equation for the electrical conductivity will be developed here.

The electrical conductivity of gasses[10,17] in electrostatic units is

$$\sigma = \frac{e^2n_e}{mc\sum_j n_jQ_j}. \tag{40}$$

To convert the unit of this electrical conductivity to Siemens per centimeter, divide it by $c^2 \times 10^{-9}$, where c is the speed of light in centimeters per second or by multiplying it by $4\pi\varepsilon_o$. e is the charge of the electron in Statcoulombs, n_e is the number of free electrons per cubic centimeter, m is mass of the electron in grams, and C is the root mean square of the electron speed having a Maxwell-Boltzmann speed distribution

$$C = \sqrt{\frac{3kT}{m}}, \tag{41}$$

where k is the Boltzmann constant in ergs per Kelvin. Substituting this into the Eq. 41 gives

$$\sigma = \frac{e^2}{c^2 \times 10^{-9}\sqrt{3mk}} \frac{n_e}{T^{\frac{1}{2}} \sum_j n_j Q_j} = 4.179 \times 10^{-10} \frac{n_e}{T^{\frac{1}{2}} \sum_j n_j Q_j} \tag{42}$$

for the conductivity in Siemens per centimeter. The summation is over the products of the number density for a component of the gas and the cross section for electron collision with the component. The components for air would be molecules, atoms, and ions of nitrogen, oxygen, and so forth. The summation is broken into 2 terms.

$$\sum_{j=0} n_j Q_j = 2.0 \times 10^{-15} n_0 + \sum_{j=1} n_j Q_j . \tag{43}$$

The first term is the assumed cross section in square centimeters for the electrons colliding with neutral atom or molecule multiplied by the number of "air atoms" even when they are bonded in molecules. This term implies that the cross section for a diatomic air molecule is about twice that of the atom in the molecule, which is a reasonable approximation. The second term is the product of the cross section and the number density of the ions having a charge *j: j* = 1 for singly charged ions, *j* = 2 for doubly charged ions, and so forth. The second term is found by assuming that all of the atoms are completely ionized and equating the conductivity to electrical conductivity of an ionized gas according to Spitzer and Harm[10]:

$$\sigma = \frac{2mC^3}{e^2 \, \mathrm{Z} \ln\left(qC^2\right)} \left(\frac{2}{3\pi}\right)^{3/2} \gamma_E\left(Z\right), \tag{44}$$

where Z is the mean ionic charge (Eq. 31). After equating the 2 conductivities, Eqs. 40 and 44 with $n_0 = 0$, the summation is

$$\sum_{j=1} n_j Q_j = \frac{e^4 n_e \, \mathrm{Z} \ln(qC^2)}{2m^2C^4} \left(\frac{3\pi}{2}\right)^{3/2} \frac{1}{\gamma_E(Z)} . \tag{45}$$

After substituting the expression for the root mean square of the velocity and collecting the constants,

$$\sum_{j=1} n_j Q_j = \left(\frac{e^4}{18k^2} \left(\frac{3\pi}{2} \right)^{3/2} \right) \frac{1}{\gamma_E(Z)} \frac{n_e \, Z \ln\left(qC^2\right)}{T^2}, \tag{46}$$

and, evaluating them,

$$\sum_{j=1} n_j Q_j = \frac{1.58689 \times 10^{-6}}{\gamma_E(Z)} \frac{n_e \, Z \ln\left(qC^2\right)}{T^2}. \tag{47}$$

The γ_E (Z) comes from the electron-electron collisions, and it too is a function of the mean ionic charge Z[18,19]:

$$\gamma_E(Z) = \left(\frac{3\pi}{32} \right) \frac{1 + 2.966Z + 0.753Z^2}{1 + 1.198Z + 0.222Z^2} \, . \tag{48}$$

A $\gamma_E = 0.567$ would give the 2.8×10^{-6} coefficient in Eq. 37, which is close to 0.574 when Z = 1 in Eq. 48. The value for qC^2 depends on the integration over the impact parameter of the collision. The upper limit of the integral, however, logarithmically approaches infinity and must be cut off at some distance. The lower limit of the integral is undefined for a zero-impact parameter. Cohen et al.[20] used the Debye's shielding radius for the upper limit where the distribution of the electrons and ions beyond this distance has little influence on the collision. The lower limit of the integral is taken to be the classical distance for closest approach of the electron to the ion. Evaluating the integral with these limits gives

$$qC^2 = \frac{3}{e^3 \sqrt{\pi n_e}} \left(\frac{kT}{2} \right)^{3/2} . \tag{49}$$

Thus, the electrical conductivity is

$$\sigma = \frac{4.179 \times 10^{-10} \, n_e T^{3/2}}{\left(2.0 \times 10^{-15} n_0 T^2 + 1.158689 \times 10^{-6} n_e \, Z \, ln\left(qC^2\right) / \gamma_E(Z) \right)}, \tag{50}$$

or when using the fractions from the equation of state,

$$\sigma = \frac{4.179 \times 10^{-10} A_0 A_1 \left(1 + A_2\right) T^{3/2}}{\left(2.0 \times 10^{-15} T^2 \left(1 - A_0 A_1\right) + 1.158689 \times 10^{-6} A_0 A_1 \left(1 + 3A_2\right) ln\left(qC^2\right) / \gamma_E(Z) \right)}, \tag{51}$$

where qC^2 and γ_E(Z) are given in the Eqs. 48 and 49.

If the interionic distance is used as the cut-off distance, instead of the Debye shielding radius, the term would be

$$q'C^2 = \frac{4kT}{e^2 n_e^{1/3}} \tag{52}$$

for singly charged ions, as cited by Cohen et al.[20] and used in Eqs. 37 and 39. The average cross section for Plooster's[4] Eq. 39 has the square of the mean ionic charge Z, but Eq. 46 has the mean ionic charge to the first power. Since the mean ionic charge is close to 1.0 for most of the conditions considered here, this difference is inconsequential. Figure 6 compares the electrical conductivities of the 2 equations as function of the temperature for various densities that occur in the calculations $0.01\rho_o$, $1.0\rho_o$, and $10.0\rho_o$.

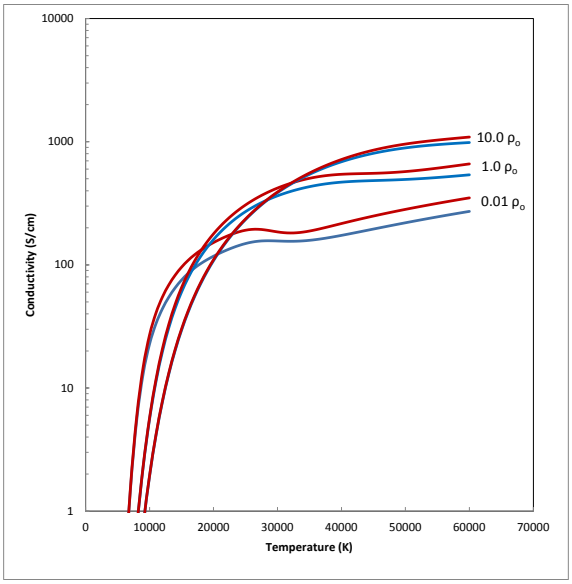

Fig. 6 Electrical conductivity by Eq. 36 (—) and Eq. 50 (—)

5. Photoionization

The photoionization of air by a black body radiator is presented by a simple example. Let a black body radiator be a cylinder with a temperature T_b and a radius R_b that has a layer of air next to it. The layer of air has a temperature T_a, density ρ, and thickness s. Assume that the temperature of the black body and the air are initially the same. At some time let the temperature of the black body be suddenly increased to a higher temperature when the 2 regions are no longer in thermal equilibrium. The photons from the black body can now ionize more air to increase the number density of free electrons, and these electrons or photoelectrons have an energy distribution. Thus, the photoelectrons can change the electrical conductivity of the air, and this change depends on time. The production rate of the photoelectrons and their energy distribution can be estimated by looking at the details for photoionization.

When a photon that has energy *(hv)* greater than the ionization potential of an atom *(ip)* is absorbed by the atom, the atom ejects a photoelectron with energy *(hv–ip)* to become a singly charged ion in its ground state. *h* is Planck's constant, and *v* is the frequency of the photon, $P_{(hv)} + A \rightarrow A^{+} + e^{-}_{(hv-ip)}$.

The probability of a photon being absorbed by an atom or molecule and producing a photoelectron is related to a cross section that depends on the energy of the incident photon. It is possible that the singly charged ion may be in an excited state after ejection of the photoelectron with even less energy. It is also possible that an atom absorbs a photon at some energy to become an atom in an excited state that later decays by ejecting an electron (autoionization). For air, however, a photon may also be absorbed by a molecule that has additional mechanisms to produce a photoelectron with less energy. The molecule may become a molecular ion, dissociate into an atom in the ground state or an excited state and an ion, and so forth. These latter mechanisms are not specifically addressed but they are indirectly included here by using the total cross section, which includes all these mechanisms. Unfortunately, the literature gives these cross sections in different units as functions of the frequency, or the energy, or the wave number, or the wave length of the photon. Also, the cross sections are given as smooth line graphs, data point graphs, or listed in tables.

In the following sections, the cross sections for the photoionization of the nitrogen molecule (N_2), nitrogen atom (N), oxygen molecule (O_2), and oxygen atom (O) are presented in units of Megabarn (Mb) as functions of the photon energy in electron volts (eVs). One Mb is 10^{-18} cm^2. Linear interpolation was used to find the cross sections on a common energy scale, as shown in Fig. 7. The total photoionization cross section for N_2[21] and O_2[22] is the production of a photoelectron with any energy leaving the molecule in any possible state: molecular ion in any of its states, dissociated atom and ion, and so forth. The total photoionization cross section for N[23] and O[24] includes the ions in an excited state. Some structure in these cross sections due to the autoionization of a highly excited atom was ignored. Note that the cross sections for the molecules are approximately twice that of their corresponding atomic cross sections.

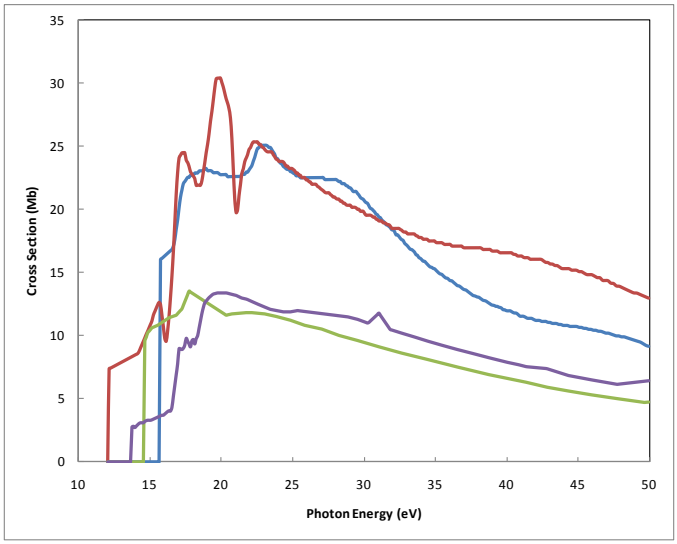

Fig. 7 Total photoionization cross sections, N_2 (—), O_2 (—), N (—), and O (—)

These cross sections were used to find the energy distribution of the photoelectrons when the source of the photons is a black body radiator. This energy distribution may be related to a temperature. As an example in finding this energy distribution, assume that the energy of the photons is 25 eV, and assume that the air is all dinitrogen and dioxygen. If the photoelectron came from dinitrogen, its energy would be 25 eV minus the ionization potential of dinitrogen (15.60 eV), or 9.40 eV. If the photoelectron came from dioxygen, however, its energy would be 25 eV minus 12.07 eV, the ionization potential of dioxygen, which would be 12.93 eV. There will be photoelectrons with less energy if the molecular ion is excited or if the molecular ion dissociates. These photoelectrons are ignored, since the number of these lesser energetic photoelectrons are smaller, because the cross sections are smaller. The energies are weighted by their respective cross section and by their fractional number in air to find their average energy.

$$E_{avg}\left(h\nu\right)=\frac{0.788\left(h\nu-15.60\right)Q_{N2}\left(h\nu\right)+0.212\left(h\nu-12.07\right)Q_{O2}\left(h\nu\right)}{\bar{Q}\left(h\nu\right)}, \quad (53)$$

where

$$\bar{Q}\left(h\nu\right)=0.788\ Q_{N2}\left(h\nu\right)+0.212\ Q_{O2}\left(h\nu\right) \quad (54)$$

is an average cross section. The 0.788 factor is the numerical fraction for the dinitrogen having a cross section $Q_{N2}(h\nu)$, and 0.212 is the numerical fraction for the dioxygen having a cross section $Q_{O2}(h\nu)$. The trace gasses in air, argon, carbon dioxide, and so forth, are excluded: If the photon energy is less than an ionizing potential, the respective cross section is zero.

When the air is exposed to the black body radiator, the production rate of photoelectrons with this average energy within a small range of energies *d(hv)* per unit volume per unit time is

$$\dot{E}\left(h\nu\right) = E_{avg}\left(h\nu\right) N_m \bar{Q}\left(h\nu\right) P\left(T_b, h\nu\right) d\left(h\nu\right), \tag{55}$$

where N_m is the number density of the dinitrogen and dioxygen of this reduced air. At a temperature of 300 K and a density 1.17681×10^{-3} g/cm^3, the number density N_m, is 2.44629×10^{19} 1/cm^3. The total number of photons within the energy range *d(hv)* that are emitted from a unit area per solid angle from the black body's surface at a temperature of T_b per unit time is

$$P\left(\nu, T_b\right) = \frac{1}{h\nu}\left[\frac{2h\nu^3}{c^2}\frac{d\nu}{\exp\left(\frac{h\nu}{kT_b}\right)-1}\right]. \tag{56}$$

The expression in the brackets is for the energy emitted in a frequency interval *dv* per unit area per unit time. Dividing this by the energy of the photon *hv* gives the number of photons per unit area per unit time, which can then be expressed as a function of the photon energy.

$$P\left(h\nu, T_b\right) = \frac{2}{c^2 h^3}\left(\frac{\left(h\nu\right)^2}{\exp\left(\frac{h\nu}{kT_b}\right)-1}\right) d\left(h\nu\right). \tag{57}$$

Thus the overall average energy is

$$\bar{E}\left(T_b\right) = \frac{\int_{h\nu_o}^{\infty} E_{avg}\left(h\nu\right)\bar{Q}\left(h\nu\right)\, P\left(h\nu, T_b\right)\, d(h\nu)}{\int_{h\nu_o}^{\infty} \bar{Q}(h\nu)\, P\left(h\nu, T_b\right)\, d(h\nu)}. \tag{58}$$

The N_m factor cancels out in this ratio. This energy average is then equated to a temperature by

$$\bar{E}\left(T_b\right) = \frac{m\overline{v^2}}{2} = \frac{m}{2}\left(\frac{3kT_e}{m}\right) \tag{59}$$

for the equivalent temperature for the photoelectrons even though their energy distribution is not a Maxwell-Boltzmann distribution.

$$T_e\left(T_b\right) = \frac{2\bar{E}\left(T_b\right)}{3k}. \tag{60}$$

The integrals used the published cross sections (Fig. 7), up to a photon energy of 50 eV, where the photon number flux is small even when the black body temperature is 60,000 K. The results are shown in Fig. 8 along with the result, where it is assumed that the air is all atomic. For all atomic air, the ionization potential for N (14.53 eV), O (13.62 eV), and their total photoionization cross sections were used to find the equivalent temperature for their photoelectrons. The black body temperature is included for comparison.

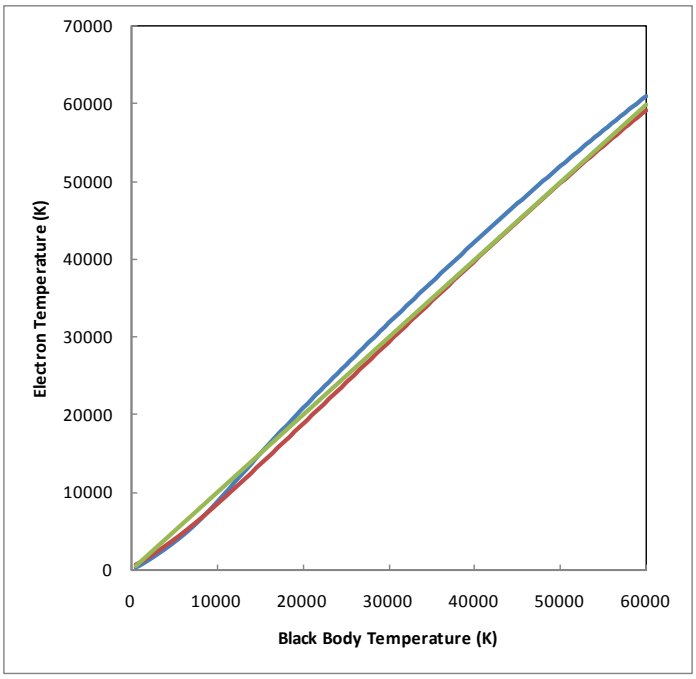

Fig. 8 Molecular air (—), atomic air (—), and black body temperature (—)

Since electron temperature is nearly equal to the black body temperature when the air is all atomic or all molecular, the electron temperature will be set equal to the black body temperature for the electrical conductivity.

The production rate of the free charges in the thick layer is found by first defining a small volume that is a right cylinder with a cross sectional area a and a length δ. At one end of the cylinder, let a number of photons $\dot{N}_p(0, h\nu)$ with an energy $h\nu$ per energy bandwidth $d(h\nu)$, per unit area, and per unit time cross perpendicular to the area a. If the layer has a uniform number density of neutral atoms or molecules N, the production rate for the photoelectrons per photon energy in this volume is

$$\dot{N}_e(h\nu) = \dot{N}_p(0, h\nu)\, N\, Q(h\nu)\, a\, \delta, \tag{61}$$

where Q is a cross section. Since for every photon that is absorbed there is a photoelectron, the number of photons leaving the cylinder at the other end is

$$\dot{N}_p(\delta, h\nu)a = \dot{N}_p(0, h\nu)a - \dot{N}_p(0, h\nu)N\,Q(h\nu)a\;\delta \tag{62}$$

for

$$\frac{\dot{N}_p(\delta, h\nu) - \dot{N}_p(0, h\nu)}{\delta} = -\dot{N}_p(0, h\nu)\;N\;Q(h\nu). \tag{63}$$

Taking the limit of δ approaching zero on the left side, this equation becomes

$$-\frac{\partial \dot{N}_p(h\nu)}{\partial \delta} = \dot{N}_p(0, h\nu)\;N\;Q(h\nu) = \frac{\dot{N}_e(h\nu)}{a\;\delta} = \dot{n}_e(h\nu) \tag{64}$$

for the number of photoelectrons being produced per unit volume per unit time. Finally, let the number distribution of the photons be proportional to the number distribution of the black body photons that can photoionize.

$$\dot{N}_p(0, h\nu) = \alpha\; P(h\nu, T_b),$$

where α includes an attenuation factor and a solid angle factor. Thus, a production rate factor can now be defined as

$$\dot{F}(T_b) = \int_{h\nu_o}^{\infty} \bar{Q}(h\nu)\; P(h\nu, T_b)\; d(h\nu) \tag{65}$$

and

$$\dot{n}_e(T_b) = N\alpha\dot{F}(T_b) \tag{66}$$

for the total photoelectron production rate per volume, where N is the number density of the neutral atoms even when they are molecules. Figure 9 shows that $\dot{F}(T_b)$ when it is assumed that the air is all molecular and when it is assumed that the air is all atomic. In both cases, $\dot{F}(T_b)$ is almost zero when the black body temperature is less than about 15,000 K and nearly equal at higher temperatures. Since it is expected that most of the photoionization will occur when the air is mostly molecular, however, the production rate for the molecular air was chosen and fitted to a polynomial for temperatures greater than 15,000 K,

$$\dot{F}(x) = -4.754\times10^{-16}x^5 + 5.325\times10^{-11}x^4 - 9.127\times10^{-8}x^3 + 1.664\times10^{-3}x^2 + 2.774x, \tag{65}$$

where x = T_b−15,000 when T_b is greater than 15,000 K. $\dot{F}(T_b) = 0$ when T_b is less than 15,000 K.

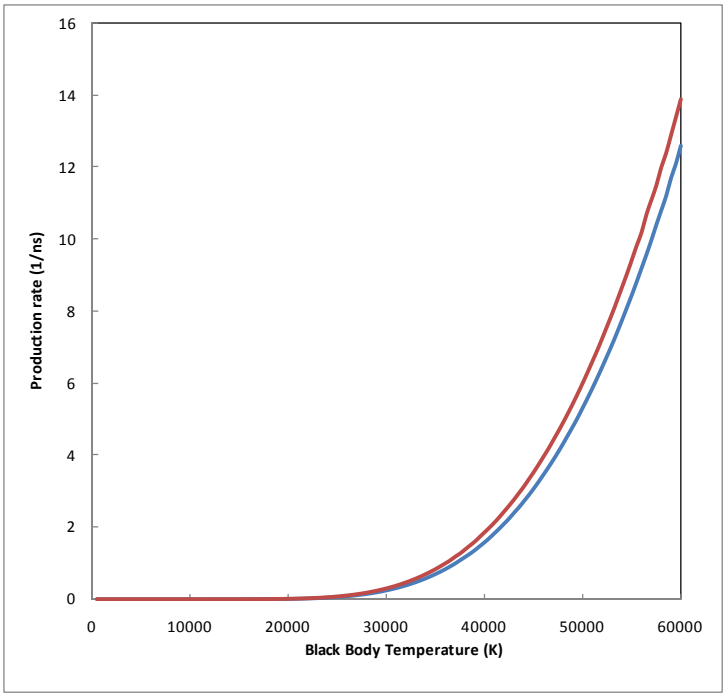

Fig. 9 Production rate for molecular air (—) and atomic air (—)

Now assume that the thickness of a cylindrical element in the arc and the mean free path of the photons are small compared with the radius of the black body R_b so that the cylindrical surface of the black body can now be taken to be a planar surface. Let the surface of a black body have an area dA_b where the photons are being emitted with a *cos* θ angular distribution and θ is the angle between the normal of the area dA_b and the travel direction of the photons. The total production rate for the photo electrons in a small volume located at a perpendicular distance s from the black body surface is

$$\dot{n}_e\left(T_b,s\right)=N\dot{F}\left(T_b\right)\left(\frac{R_b}{R_b+s}\right)\frac{\exp\left(-kr\right)cos\theta\, dA_b}{2\pi r^2}, \tag{68}$$

where k is an absorption coefficient and r is the distance from the area on the black body surface to the small volume. The factor in the parenthesizes with the radius of the black body Rb accounts for the curvature of the surface. This expression is to be integrated over the entire planar surface of the black body by using cylindrical coordinates (ρ, φ). The area dA_b is then $\rho\, d\rho\, d\varphi$.

$$\begin{aligned}\dot{n}_e\left(T_b,s\right)&=\frac{N\dot{F}\left(T_b\right)}{2\pi}\left(\frac{R_b}{R_b+s}\right)\int_0^{2\pi}d\varphi\int_0^{\infty}\rho\; d\rho\,\frac{\exp\left(-kr\right)\; cos\theta}{r^2}\\ \dot{n}_e\left(T_b,s\right)&=N\;\dot{F}\left(T_b\right)\left(\frac{R_b}{R_b+s}\right)\int_0^{\infty}\rho\; d\rho\,\frac{\exp\left(-kr\right)\; cos\theta}{r^2}\end{aligned} \tag{69}$$

for the total production rate for the photoelectrons per unit volume. The integral is evaluated by changing the variable for integration. First let $\rho\, d\rho = r\, dr$ from the differentiation of $r^2 = \rho^2 + s^2$ and $\cos\theta$ = s/r,

$$I = s\int_s^\infty dr \frac{\exp(-kr)}{r^2}, \tag{70}$$

and then let x = kr for dr = dx/k,

$$I(ks) = ks\int_{ks}^\infty dx \frac{\exp(-x)}{x^2}, \tag{71}$$

and

$$\dot{n}_e(T_b, s) = N\left(\frac{R_b}{R_b + s}\right)\dot{F}(T_b)\, I(ks). \tag{72}$$

The total production rate for the region between the black body surface and the distance s is

$$\dot{n}_e(s) = N\left(\frac{R_b}{R_b + s}\right)\dot{F}(T_b)\big(1 - I(ks)\big). \tag{73}$$

The integral $I(ks)$ was numerically integrated as a function of ks, which is the optical density of the layer. The values of the integral were fitted to an empirical formula,

$$I(ks) \cong 0.6906\exp(-1.52ks) + 0.3094\exp(-8.32ks), \tag{74}$$

that is a sufficient approximation for the integral. If it is assumed that the spectrum of the photons is proportional to the black body throughout the thick layer, then a weighted cross section may be defined by first substituting Eq. 57 for $\dot{N}_p(s, h\upsilon)$ in Eq. 64 and integrating over the photon energy,

$$-\frac{\partial}{\partial s}\int_{h\upsilon_o}^\infty P(h\nu, T_b)\, d(h\nu) = N\int_{h\upsilon_o}^\infty \bar{Q}(h\nu)\, P(h\nu, T_b)\, d(h\nu), \tag{75}$$

and then define

$$Q_b(T_b)\int_{h\upsilon_o}^\infty P(h\nu, T_b)\, d(h\nu) = \int_{h\upsilon_o}^\infty \bar{Q}(h\nu)\, P(h\nu, T_b)\, d(h\nu) \tag{76}$$

for a cross section that is weighted over the photon energy. Also let

$$\Gamma\left(T_b\right) = \int_{h\upsilon_o}^{\infty} P(h\nu, T_b)\, d(h\nu) \tag{77}$$

for the total number of photons per area per second with energies greater than $h\nu_o$. With these definitions, the equation is then

$$-\frac{\partial \Gamma\left(T_b\right)}{\partial s} = N\, Q_b\left(T_b\right)\Gamma\left(T_b\right), \tag{78}$$

where a coefficient of absorption can be defined as

$$k = N\, Q_b\left(T_b\right) = N\, \frac{\int_{h\upsilon_o}^{\infty} \bar{Q}\left(h\nu\right)\, P(h\nu, T_b)\, d(h\nu)}{\int_{h\upsilon_o}^{\infty} P(h\nu, T_b)\, d(h\nu)} \tag{79}$$

for the black body distribution. The weighed cross section per atom is shown in Fig. 10 for an all molecular air where $h\upsilon_0$ = 12.07 eV is the ionization potential of O_2. The weighted cross section for all atomic air has $h\upsilon_0$ = 13.62 eV, which is the ionization potential for atomic O.

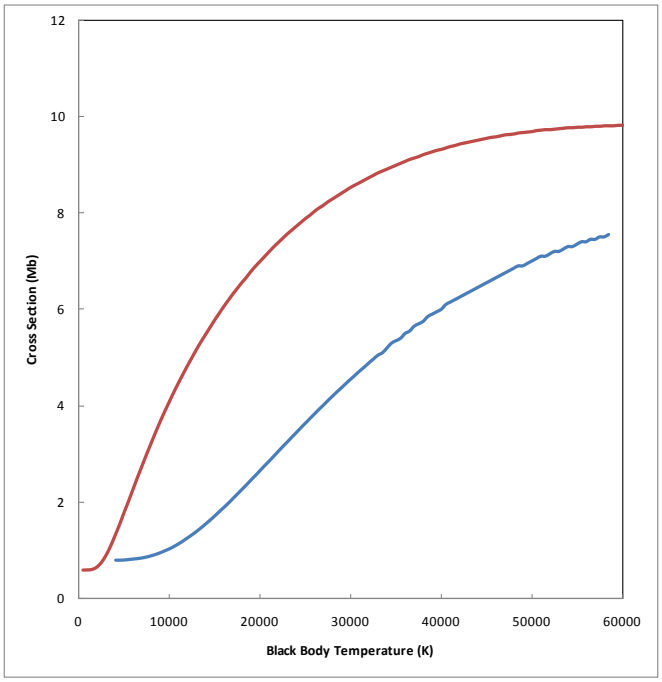

Fig. 10 Weighted cross section per atom; molecular air (——) and atomic air (——)

Since it is expected that most of the photoionization will occur when the air is mostly molecular, the weighted cross section in Megabarns was fitted to the following polynomial for temperatures greater than 4000 K,

$$Q_b(T_b) = 2.209\times10^{-18}T_b^4 - 3.398\times10^{-13}T_b^3 + 1.647\times10^{-8}T_b^2 - 1.321\times10^{-4}T_b + 1.064 \quad (80)$$

and $Q_b(T_b) = 0.778$ Mb when the temperature is less than 4000 K.

In the finite difference method for the electric arc there are a number of layers. Since these layers may have different thicknesses and different absorption coefficients to give different optical densities, determining the photon flux for each layer would be difficult when the procedure for the single layer is applied for a number of layers. Thus, an assumption is made to ease the calculation. When the photons leave the absorbing layer, they have a different angular distribution when entering the next layer. Photons having an angle close to $\pi/2$ are lessened by $\cos\theta$, and they have a long absorption path. Photons with zero angle are not lessened by $\cos\theta$, and they have a shorter absorption path. Depending on the optical density of the layer, this changes the angular distribution of the photons and attenuates the photons. Layers with low optical densities less than about 0.1, for example, have angular distributions close to that of the black body but attenuated by about 10%. Layers with high optical densities greater than about 1.0, for example, have angular distributions that are more pronounced at small angles but attenuated by about 60%. Also, since the optical density depends on the frequency of the photons, the spectrum of the photons after passing through the layer may no longer be that of a black body. Still, it is assumed that the spectrum of these photons is a black body but attenuated, and the angular distribution of the photons is the same as the black body so that these equations can be applied to the next layer.

As an example of the change in the electrical conductivity of a layer due to photoionization, a layer just outside the channel was chosen from the calculations that produced the results shown in Figs. 2–5. At a time near the peak current, 6.0 μs, a layer had the following properties: temperature (T = 2436 K), density ($\rho = 1.31\times10^{-3}$ g cm^{-3}), and width (s = 8.17×10^{-4} cm). The layer next to it was inside the channel and had a black body temperature of 34,000 K. The time step for the calculation was 1.68×10^{-9} s. The total number density of atoms and ions in the layer is $N = (1.31\times10^{-3})(6.022\times10^{23})/14.43 = 5.43\times10^{19}$ cm^{-3}, where 14.43 is taken to be an atomic weight of air. Before this layer is exposed to the black body radiation, the fractions for the components of air from Eq. 32 gives $A_0 = 2.89\times10^{-7}$, $A_1 = 5.93\times10^{-15}$, and $A_2 = 1.41\times10^{-63}$. From these fractions, the total number density for the neutral atoms even when they are in molecules is $n_0 = 5.43\times10^{19}$ cm^{-3}. The number density for the electrons is $n_e = 0.09$ cm^{-3}, and the number density for the singly charged ions is $n_1 = 0.09$ cm^{-3}. The number density for the doubly charged

ions is $n_2 = 1.3\times10^{-64}$ cm^{-3}. Thus, with the mean ionic charge Z (Eq. 35) of 1.0 and temperature of 2436 K, the electrical conductivity of the layer (Eq. 37), is 7.27×10^{-18} S/cm. Now let this layer be exposed to the black body radiation at a temperature of 34,000 K, which will produce photoelectrons with the energy equivalent to this temperature. The weighted cross section for photoionization (Eq. 80) is 5.21×10^{-18} cm^{2,} for a coefficient of absorption $k = n_0\, 5.21\times10^{-18} = 283$ cm^{-1} and an optical thickness $ks = k\, 4.49\times10^{-4} = 0.231$. The total absorption in the layer is $I(ks) = 0.531$, and the production rate is $\dot{F}(34000) = 1.784 \times 10^{8}$ s^{-1}. The total production rate for the photoelectrons per volume per second in the layer is then

$$\dot{n}_e(s) = 5.43\times10^{19}\left(1.784\times10^{8}\right)(1-0.531) = 4.54\times10^{27} \qquad (81)$$

when the radius of the black body R_b is larger than the thickness of the layer. After the time step of 1.68×10^{-9} s, the number density of the photo electrons is $n_e = 4.54\times10^{27}$ (1.68×10^{-9}) for $n_e = 7.63\times10^{18}$ cm^{-3}. The number density of the neutrals is $n_0 = 5.43\times10^{19} - n_e$ for $n_0 = 4.67\times10^{19}$ cm^{-3}, and the number density of singly charged ions is $n_1 = 0.09 + n_e$ for $n_1 = 7.63\times10^{18}$ cm^{-3}. The number density for the doubly charged ions does not change. The mean ion charge is still Z = 1 because the number density for the doubly charged ions is very small. Using these number densities and an electron temperature of 34,000 K, the conductivity is 117 S/cm, which is to be added to the electrical conductivity before photoionization: 7.27×10^{-18} S/cm. In other parts of the arc, the conductivities before and after photoionization are comparable. Thus, the total of the conductivities in this case is 117 S/cm, while a typical electrical conductivity in the channel is 200 S/cm.

This chosen layer, however, is also being photoionized by an attenuated flux of photons from other more-distant layers having different temperatures where the temperature of these photoelectrons are set to be equal to the temperature of the distant layer. The attenuation of the photon flux from a distant layer is determined by following the attenuation through each intervening layer having an optical thickness and a value for $I(ks)$. This attenuated flux is used for an additional production rate for the photoelectrons in the layer. The total production rate is multiplied by the time step for the number density of the photoelectrons that are added to the free electrons in the layer. A like number is added to the number density of the singly charged ions and subtracted from the number density of atoms. The number density for the doubly charged ions is not changed. Since it is assumed that the spectrum from the distant layer is a black body, the temperature of these photoelectrons is equal to the temperature of the distant layer. An average electron

temperature in the *i*th layer produced by all the distant layers *(i ≠ j)* may be defined by a weighted average,

$$\overline{T}_i = \frac{\sum_{j\neq i} T_j \left(\dot{n}_e\right)_{i,j}}{\sum_{j\neq i} \left(\dot{n}_e\right)_{i,j}}, \tag{82}$$

where the added half integer for the indexes of these intrinsic properties is dropped. This temperature is then used to define a temperature for all of the photoelectrons by 2 sums. Let the first summation be

$$\mathrm{S}_i^n = \mathrm{S}_i^{n-1} + \overline{T}_i \left(\dot{n}_e\right)_i \Delta t_n, \tag{83}$$

which is a sum of the product of the average temperature of the newly produced photoelectrons and their number. The second summation is the number of the newly produced photoelectrons,

$$\mathrm{D}_i^n = \mathrm{D}_i^{n-1} + \left(\dot{n}_e\right)_i \Delta t_n. \tag{84}$$

Δt_n is the time step and $\left(\dot{N}_e\right)_i$ is the total production rate of the additional photoelectrons by all the other elements. Thus, the average temperature for all photoelectrons may be defined as

$$\overline{\overline{T}}_i = \frac{S_i^n}{D_i^n}. \tag{85}$$

During this time, however, all of the photoelectrons in an element may be recombining with the ions. When an electron comes close to an ion, the electron could lose energy when a photon is emitted and recombine with the ion. This sequence is the time reverse of photoionization. The cross section for recombination for hydrogen-like atoms[13] as a function of the speed of the electrons v_e is

$$\sigma_c \cong \frac{1.1\times 10^{-5}}{v_e^2}, \tag{86}$$

where the cross section is in square centimeters. Although the ions are not hydrogen, the upper energy levels of the oxygen and nitrogen ions, where most of the electrons will recombine, are hydrogen-like. The recombination rate per unit volume and per unit time for electrons with a velocity v_e is

$$\dot{N}_c = n_e n_1 \sigma_c v_e. \tag{87}$$

n_e is the number density of the electrons and n_1 is the number density of the singly charged ions. If the electrons have a Maxwell velocity distribution for a temperature $f(v_e,T)$, the weighted recombination rate for the electrons is

$$\dot{R}_c = 1.1\times10^{-5} n_e n_1 \int_0^\infty dv_e \frac{f(v_e,T)}{v_e} = \frac{2.2\times10^{-11} n_e n_1}{\sqrt{T_i}} . \tag{88}$$

Thus, at the end of the time step, the number density in the element for the electrons, neutrals, and singly charged ions are

$$\begin{aligned} n_e^n &= n_e^{n-1} + \left(\dot{n}_e - \dot{R}_c\right)\Delta t_n \\ n_0^n &= n_0^{n-1} - \left(\dot{n}_e - \dot{R}_c\right)\Delta t_n \\ n_1^n &= n_1^{n-1} + \left(\dot{n}_e - \dot{R}_c\right)\Delta t_n \end{aligned} , \tag{89}$$

where the index for the element is dropped and the recombination with the doubly charged ions are ignored. The number densities for the neutrals and the singly charged ions must be greater than zero but less than the total number density N. The number density for the electrons can be greater than the total number density when there are doubly charged ions present. These limits are enforced at the end of each time step.

6. Results

The finite difference equations (Eqs. 8–16) were solved using Eq. 28 for the thermal conductivity for 2 cases. The initial condition for each case has the air within a radius of 0.1 cm with a temperature of 15,000 K at ambient density. The total conductivity of the arc (Fig. 11) was calculated for a current given by Eq. 21. The first case has no production of the photoelectrons (no PEs) and Eq. 50 for the electrical conductivity. The second case has the PEs and Eq. 50 for the electrical conductivity. The temperature and pressure at the center of the arc, the radius of the channel, and the position of the shock wave are compared with Akram's results,[7,8] which include radiation transfer. Fig. 11 is the conductivity of the arc as a function of time when there is photoionization (PE) and when there is no photoionization (no PE). When there is photoionization, the atoms in the channel quickly become completely ionized, which results in making the channel more conductive. The total conductivity using Eq. 36 and no PE is also shown to simulate Akram's results.

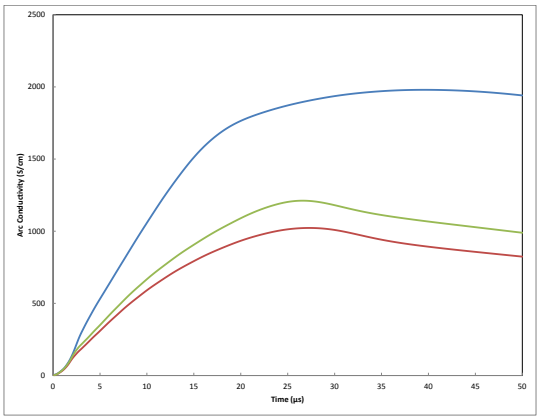

Fig. 11 Conductivity of the arc: PE (——), no PE (——), and Eq. 36 (——)

The temperature at the center of the arc, x = 0 (Fig. 12) tends to decrease as the electrical conductivity increases. This is reasonable because an increase in the conductivity results in a decrease in the Joule heating for a given current. The temperature by Akram,[7,8] also in Fig. 12, follows this trend. The electrical conductivity used by Akram (Fig. 6) is generally higher than Eq. 50, and presumably the inclusion of radiation transfer by Akram would also increase the conductivity. In comparison, using Eq. 50 with no production of photoelectrons resulted in a high core temperature.

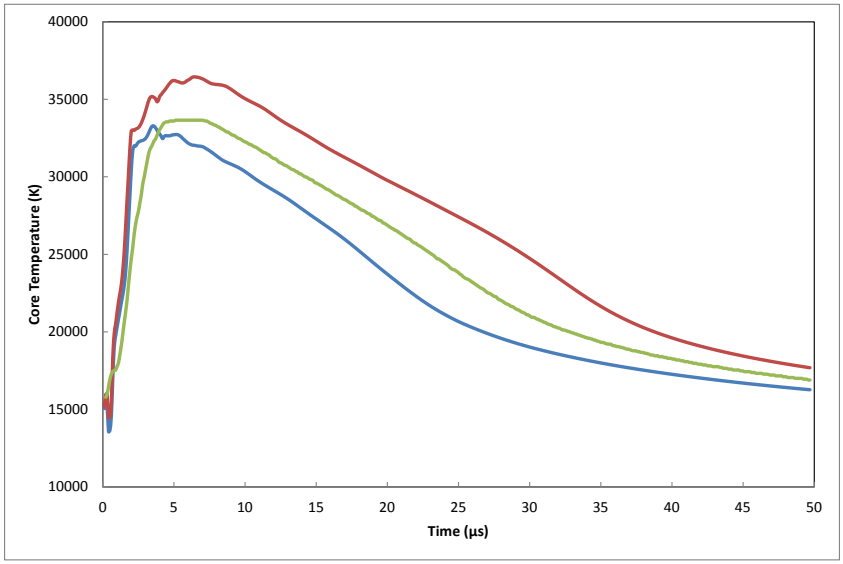

Fig. 12 Core temperature: PE (——), no PE (——), and Akram[7] (——)

The pressure at the center of the arc (Fig. 13) seems to be insensitive to the photoelectrons. In the case where there are no photoelectrons, the pressure agrees with the pressure according to Akram.

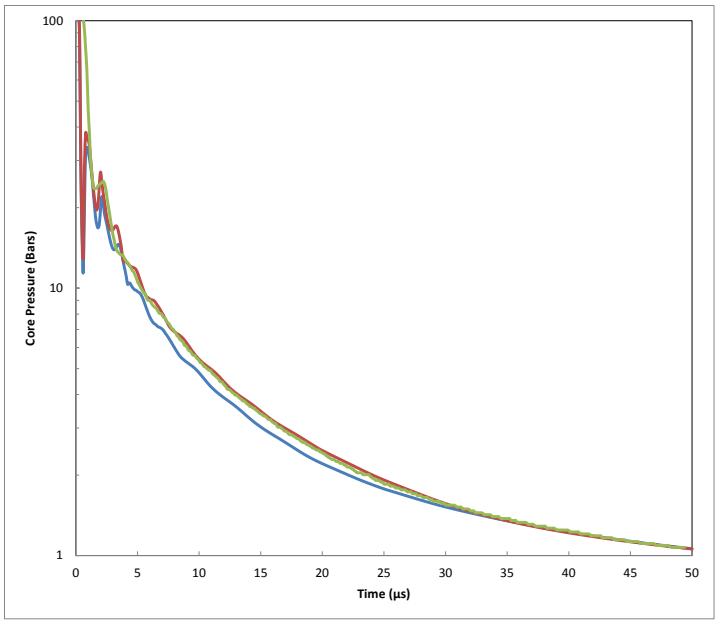

Fig. 13 Core pressure: PE (—), no PE (—), and Akram[7,8] (—)

Figure 14 shows the radius of the channel and the position of the shock wave during the current pulse. The radius of the channel is taken as the radius where the temperature is half of the temperature at the very center (Fig. 2). The position of the shock wave is where there is the maximum pressure (Fig. 3). The position of the shock wave and the radius of the channel are again close to Akram's results when there are no photoelectrons. These radii are slightly reduced when photoelectrons are included because of the reduced Joule heating of the channel due to its high conductivity.

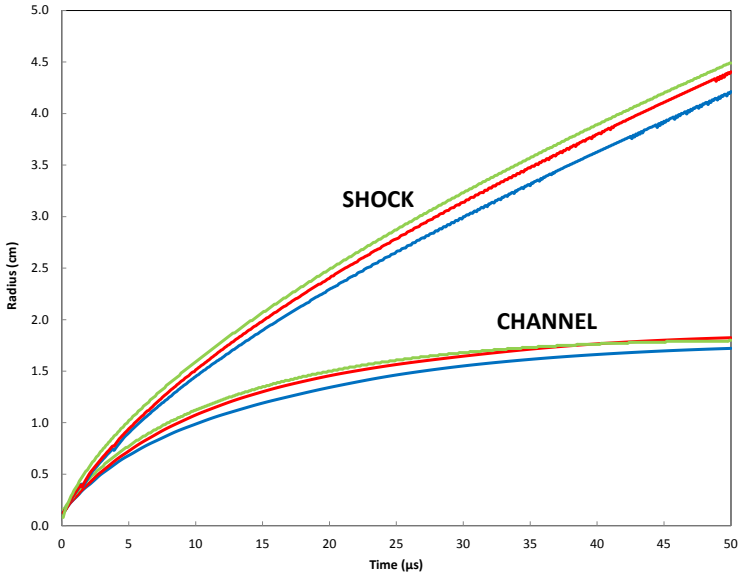

Fig. 14 Radius of the channel and shock wave: PE (—), no PE (—), and Akram[7,8] (—)

Except for the core temperature, when there is no photoionization, the present results agree with Akram's results. Using the lower conductivity and omitting the photoionization that gave a higher core temperature for these seems to be comparable to the higher conductivity and the radiation transfer in Akram's results. When the photoionization was included, the core temperature was reduced and the conductivity of the arc increased. Photoionization, however, had little effect on the pressure at the center, the radius of the channel, and the position of the shock wave.

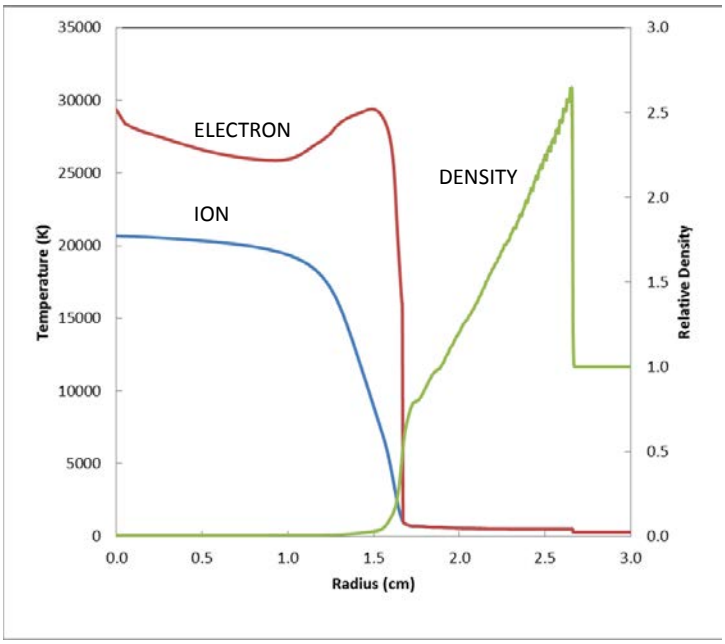

Fig. 15 Ion temperature (—), electron temperature (—), and relative density (—) at 25 μs

When there is photoionization, the temperature of the electrons is different from the temperature of the ions and atoms. Figure 15 is a profile of the electron temperature and the ion temperature, which includes the atoms as well. The relative density of air is also included with its scale on the right side. These profiles are at a time of 25 μs when high-temperature electrons in dense air are evident. The number density of these electrons, however, are relatively low, but the conductivity of the air is sufficient for Joule heating to be noticeable at the radius of about 1.7 cm.

7. Conclusion

The results of this study evaluated quantities that are accessible to measurement and whether they can be used to infer the mechanisms in the arc. The radius of the conducting channel can be measured by laser interferogram.[3] The peak pressure of the shock wave can be measured and its position can be sensed by pressure sensors. These quantities, however, are nearly identical in 2 cases. In the first case,[7] the

electrical conductivity was generally larger than the one given by Eq. 50 and included radiation transfer. The second case used Eq. 50 for the electrical conductivity and did not include radiation transfer and no photoionization (no PE). Thus, these measurements may not distinguish the 2 cases. The temperature at the very center is different, but this temperature is not assessable to measurement. The total conductivity of the arc, however, is different and assessable to measurement that can distinguish these 2 cases. Since the total conductivity of the arc conductivity is even higher than these cases when photoionization is included (PE), the effects of photoionization can be evaluated. Determining the high conductivity of an arc is difficult because it requires careful measurements and analysis of the current, the voltage across the arc, and the radius of the arc.

It was assumed in the previous studies that a finite element radiates as a black body. This assumption was used here so that the present results can be compared with previous calculations. A number of assumptions were made to ease the calculation of the radiation transfer via photoionization while other processes were ignored. This assumption resulted in different temperatures for the ions and electrons. Eventually, these temperatures should tend to become equal to reach thermal equilibrium. Thus a more detailed description of the radiation transfer and the other processes will be included in the future.

8. References

1. Engel TG, Donaldson AL, Kristiansen M. The pulsed discharge arc resistance and its functional behavior. IEEE Transactions on Plasma Science. 1989;17(2):323–329.

2. Akiyama H, Kristiansen M, Krompholz H, Maas B. Current-voltage characteristics of a high-current pulsed discharge in air. IEEE Transactions on Plasma Science. 1988;16(2):312–316.

3. Kushner MJ, Kimura WD, Byron SR. Arc resistance of laser-triggered spark gaps. J Appl Phys. 1985;58(5):1744–1751.

4. Plooster MN. Numerical simulation of spark discharges in air. The Physics of Fluids. 1971;14(16):2111–2123.

5. Plooster MN. Shock waves from line sources: numerical solutions and experimental measurements. The Physics of Fluids. 1970;13(11):2665–2675.

6. VonNeumann J, Richtmyer RD. A method for the numerical calculation of hydrodynamic shocks. J Appl Phys. 1950;21:232–237.

7. Akram M, Lundgren E. The evolution of spark discharges in gases: I. macroscopic models. J Phys D Appl Phys. 1996;29:2129–2136.

8. Akram M. The evolution of spark discharges in gases: II. numerical solution of one-dimensional models. J Phys D Appl Phys. 1996;29:2137–2146.

9. Olsen HN. Thermal and electrical properties of an argon plasma. Physics of Fluids. 1959;2(6):614–623.

10. Spitzer L, Harm R. Transport phenomena in a completely ionized gas. Physical Review. 1953;89(5):977–981.

11. Riviere PH, Soufiani A, Perrin MY, Riad H, Gleizes A. Air mixture radiative property modelling in the temperature range 10,000–40,000 K. J Quant Spectrosc Radiat Transfer. 1996;56(1):29–45.

12. Chauverau S, Deron C, Perrin M, Riviere P, Soufiani A. Radiative transfer in LTE air plasmas for temperatures up to 15,000 K. J Quant Spectrosc Radiat Transfer. 2003;77:113–130.

13. Zeldovich YB, Raiser YP. Physics of shock waves and high-temperature hydrodynamic phenomena. In: Hayes WD, Probstein RF, editors. Temperature hydrodynamic phenomena. Mineola (NY): Dover Publications, Inc.; 2002.

14. Press WH, Flannery BP, Teukolsky SA, Vetterling WT. Numerical recipes. (London): Cambridge University Press; 1986.

15. Plooster MN. Shock waves from line sources. Boulder (CO): National Center for Atmospheric Research; 1968 Nov. Report No.: NCAR-TN-37.

16. Richtmyer RD, Morton KW. Difference methods for initial value problems. 2nd ed. New York (NY): Interscience; 1994. p. 405.

17. Lamb L, Lin S. Electrical conductivity of thermally ionized air produced in a shock tube. J Appl Phys. 1957;28(7):754.

18. Hirshman SP. Transport of a multiple ion species plasma in the Pfirsch-Schluter regime. Physics of Fluids. 1977;20(4):589–598.

19. Callen JD. Fundamentals of plasma physics. Draft; 2003 [accessed 2016 July 26]. http://homepages.cae.wisc.edu/~callen/book.html.

20. Cohen RS, Spitzer L, Routly PM. The electrical conductivity of an ionized gas. Physical Review. 1950;80(2):230–238.

21. Itikawa Y, Hayashi A, Ichimura K, Onda K, Sakimoto K, Takayanagi K, Nakamura M, Nishimura H, Takayanagi T. Cross sections for electrons and photons with nitrogen molecules. J Phys Chem Ref Data. 1986;15(3):985–1010.

22. Itikawa Y, Ichimura A, Onda K, Sakimoto K, Takayanagi K, Hatano Y, Hayashi M, Nishimura H, Tsurubuchi S. Cross sections for collisions of electrons and photons with oxygen molecules. J Phys Chem Ref Data. 1989;18(1):23–42.

23. Samson JAR, Angel GC. Single- and double-photoionization cross sections of atomic nitrogen from threshold to 31 A. Physical Review A. 1990;42(1):1307–1312.

24. Angel GC, Samson JAR. Total photoionization cross sections of atomic oxygen from threshold to 44.3 Å. Physical Review A. 1988;38(11):5578–5585.

List of Symbols, Abbreviations, and Acronyms

1-D	1-dimensional
eV	electron volt
Mb	Megabarn
N	nitrogen atom
N_2	nitrogen molecule
no PE	no photoelectrons produced
O	oxygen atom
O_2	oxygen molecule
PE	photoelectrons produced

1 (PDF) DEFENSE TECHNICAL INFORMATION CTR DTIC OCA

2 (PDF) DIRECTOR US ARMY RESEARCH LAB RDRL CIO L IMAL HRA MAIL & RECORDS MGMT

1 (PDF) GOVT PRINTG OFC A MALHOTRA

1 (PDF) DIR USARL RDRL WMP A C HUMMER